Particuology 25 (2016) 111–121

Contents lists available at ScienceDirect

Particuology

journal homepage: www.elsevier.com/locate/partic

# DEM investigation on the effect of sample preparation on the shear behavior of granular soil

Beibing Dai[a,*], Jun Yang[b], Cuiying Zhou[a], Xiaodong Luo[b]

[a] Research Institute of Geotechnical Engineering and Information Technology, Sun Yat-sen University, China
[b] Department of Civil Engineering, The University of Hong Kong, Hong Kong, China

ARTICLE INFO

*Article history:*
Received 17 September 2014
Received in revised form 3 March 2015
Accepted 16 March 2015
Available online 8 September 2015

*Keywords:*
Initial fabric anisotropy
Stress–dilatancy relationship
Shear strength
Critical state line
Particle motion

ABSTRACT

The effect of initial fabric anisotropy produced by sample preparation on the shear behavior of granular soil is investigated by performing discrete element method (DEM) simulations of fourteen biaxial tests in drained conditions. Numerical test specimens are prepared by three means: gravitational deposition, multi-layer compression, and isotropic compression, such that different initial inherent soil fabrics are created. The DEM simulation results show that initial fabric anisotropy exerts a considerable effect on the shear behavior of granular soil, and that the peak stress ratio and peak dilatancy increase with an increase in the fabric index $a_n$ that is estimated from the contact orientations. The stress–dilatancy relationship is found to be independent of the initial fabric anisotropy. The anisotropy related to the contact orientation and contact normal force accounts for the main contribution to the mobilized friction angle. Also, the occurrence of contractive shear response in an initial shearing stage is accompanied by the most intense particle rearrangement and microstructural reorganization, regardless of the sample preparation method. Furthermore, the uniqueness of the critical state line in $e$–log $p'$ and $q$–$p'$ plots is observed, suggesting that the influence of initial fabric anisotropy is erased at large shear strains.



## Introduction

The current understanding of stress–strain behavior of granular soil has been achieved mainly from well-controlled laboratory tests on prepared specimens. Such specimens are generally reconstituted from natural in situ soil via different sample preparation methods, such as dry deposition, moist tamping, or moist vibration. It has been consistently observed in laboratory tests that soil specimens reconstituted by different means exhibit different mechanical behaviors (Chang, Heymann, & Clayton, 2011; Chen & Chuang, 2001; DeGregorio, 1990; Ladd, 1974; Miura & Toki, 1982; Mulilis, Arulanandan, Mitchell, Chan, & Seed, 1977; Sadrekarimi & Olson, 2012; Sze & Yang, 2014; Tatsuoka, Ochi, Fujii, & Okamoto, 1986; Vaid, Sivathayalan, & Stedman, 1999; Yang, Li, & Yang, 2008).

As shown in Fig. 1, Sze and Yang (2014) performed triaxial compression tests on Toyoura sand specimens that were prepared by dry deposition and moist tamping methods, respectively. It was found that the specimen prepared by moist tamping exhibited a markedly less dilative response as compared with that prepared by dry deposition despite the two specimens having the same effective confining stresses and similar void ratios prior to shearing. Similarly, Vaid et al. (1999) reported that a specimen of Fraser River sand prepared by moist tamping showed notably less dilative behavior than that prepared using the water pluviation method.

The effect of initial fabric anisotropy on the position of the critical state line (CSL) in plots of $e$–log $p'$ has also raised some debate. Traditionally, it was accepted that, for a given soil, a unique CSL exists (Castro, 1969; Poulos, 1981; Roscoe, Schofield, & Wroth, 1958). Several researchers (Been, Jefferies, & Hachey, 1991; Ishihara, 1993) found that the position of the CSL of sand in plots of $e$–log $p'$ was independent of the initial fabric anisotropy caused by the sample preparation, assuming that the initial fabric anisotropy would eventually be erased at large shear strains. However, the research of Chen and Chuang (2001) and Chang et al. (2011) suggests that the CSL is not necessarily unique and is dependent on the method of sample preparation.

The fabric anisotropy produced by sample preparation originates mainly from the particulate nature of the soil mass. Packing discrete soil particles in different manners is expected to result in different spatial arrangements of the particles as well as different interactions between the particles. Thus, it is of great interest to scrutinize the particle arrangements and interactions at a

* Corresponding author. Tel.: +86 2084111124.
*E-mail addresses:* beibing.dai@yahoo.com, daibb@mail.sysu.edu.cn (B. Dai).

http://dx.doi.org/10.1016/j.partic.2015.03.010

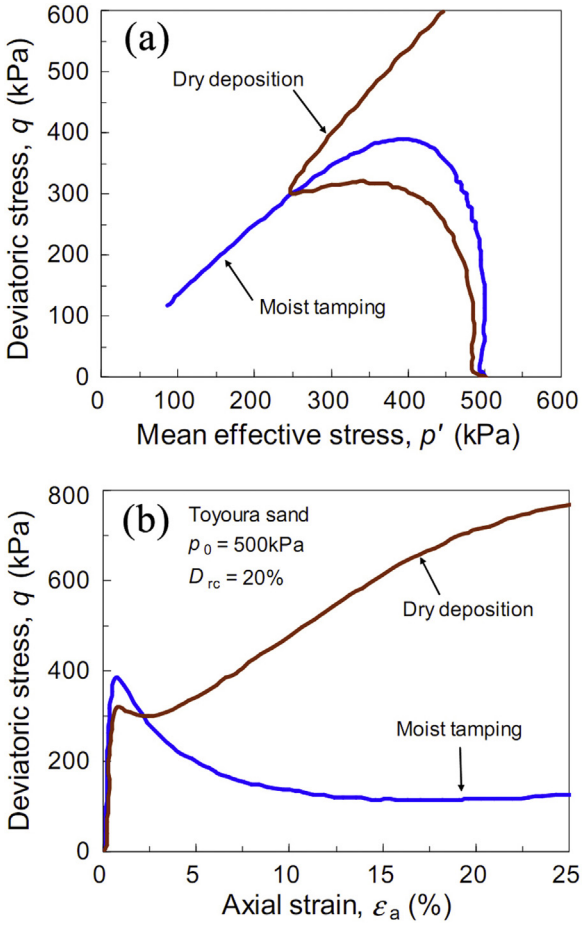


**Fig. 1.** Graphic illustration of shear behavior of specimens reconstituted by different methods: (a) $q$ vs. $p'$ and (b) $q$ vs. $\varepsilon_a$ (Sze & Yang, 2014).

microscopic scale to better understand the influence of fabric anisotropy created by sample reconstitution on shear behavior measured at the macroscopic scale.

Several researchers, such as Muhunthan, Masad, and Assaad (2000) and Yang et al. (2008), have made efforts to measure the fabric anisotropy of reconstituted soil specimens in the laboratory, but it appears to be difficult to establish a direct link between the measured fabric anisotropy and the shear behavior observed. This is because the measurement and quantification of fabric anisotropy necessitates, to a greater or lesser extent, the disturbance or even destruction of the soil specimen structure.

Ng (2004), using the discrete element method (DEM) that was pioneered by Cundall (1971), investigated the shear behavior of a series of anisotropic soil specimens prepared by different methods. He concluded that the fabric anisotropy exerted little influence on the behavior of granular soil, which is contrary to the laboratory test observations of Sze and Yang (2014) and Vaid et al. (1999). There is evidently still no conclusive link between the effects of sample preparation and shear behavior of granular soil.

This paper presents a carefully designed DEM investigation into the influence of sample preparation on the shear behavior of granular soil. Three sample preparation methods are considered in this study, including gravitational deposition, multi-layer compression, and isotropic compression. The link between fabric anisotropy generated by the sample preparation and the macroscopic shear responses (i.e., shear strength and stress–dilatancy behavior) is investigated from a micromechanical perspective. Moreover, the impact of fabric anisotropy on the position of the CSL in both $e$–log $p'$ and $q$–$p'$ plots is also examined.

## Methodology and modeling

### *Numerical modeling*

A series of biaxial tests were carried out on granular specimens with different inherent fabric anisotropy by using the computational program PFC2D (Itasca, 2005). While 3D simulations are generally preferable to 2D simulations, 3D simulations require a much higher computational cost and 2D simulations are more computationally efficient. Many published simulations have shown that various important features of the behavior of granular soil observed in the laboratory can be reasonably reproduced in 2D simulations (Dai, Yang, & Luo, 2015; Jiang, Konrad, & Leroueil, 2003; Khalili & Mahboubi, 2014; Mahmud Sazzad, 2014; Yang & Dai, 2011; Zhang & Thornton, 2007).

To allow for the natural, irregular shape of real soil particles, each particle in the numerical specimen is formed by clumping together two circular particles with an overall aspect ratio of 0.6. The particle size of such a clumped particle is equivalently estimated to be the diameter of a circular particle with the same area as that of the clumped particle, and the cumulative size distribution curve is shown in Fig. 2. The contact behavior between particles is described by the linear elastic contact model specified in PFC2D, and the friction behavior at contacts is assumed to obey the Coulomb friction law. The modeling parameters are presented in Table 1.

The granular specimens were prepared in three ways: gravitational deposition (denoted as Dep), isotropic compression (Iso), and multi-layer compression (Mult) methods. Gravitational deposition is accomplished by applying a gravity field to the domain in which the initially-generated particles are dispersed (Dai, 2010). In doing so, particles descend and are deposited onto the bottom wall of the preparation vessel. Isotropic compression (Fig. 3) is achieved by simultaneously closing the four boundary walls

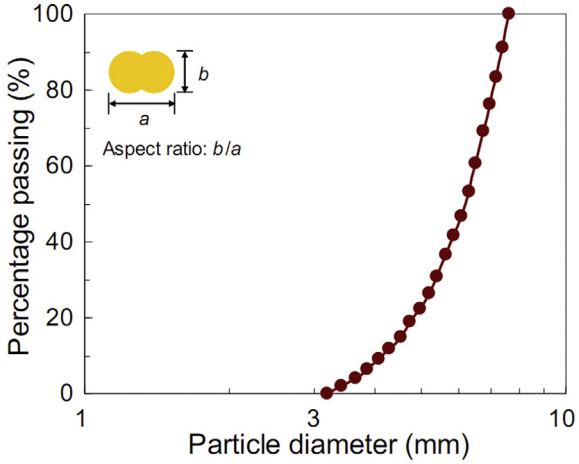


**Fig. 2.** Shape and cumulative size distribution of soil particles used in the numerical simulations.

**Table 1**
Parameters used in the DEM simulations.

| | |
|---|---|
| Particle density, $\rho$ (g/cm$^3$) | 2.65 |
| Aspect ratio, $R_a$ | 0.6 |
| Inter-particle friction, $\mu_s$ | 0.5 |
| Wall friction, $\mu_w$ | 0.0 |
| Normal and tangential stiffness, $k_n$ and $k_s$ (N/m) | $1.0 \times 10^9$ |
| Wall stiffness, $k_w$ (N/m) | $1.0 \times 10^9$ |
| Damping factor, $\alpha$ | 0.7 |

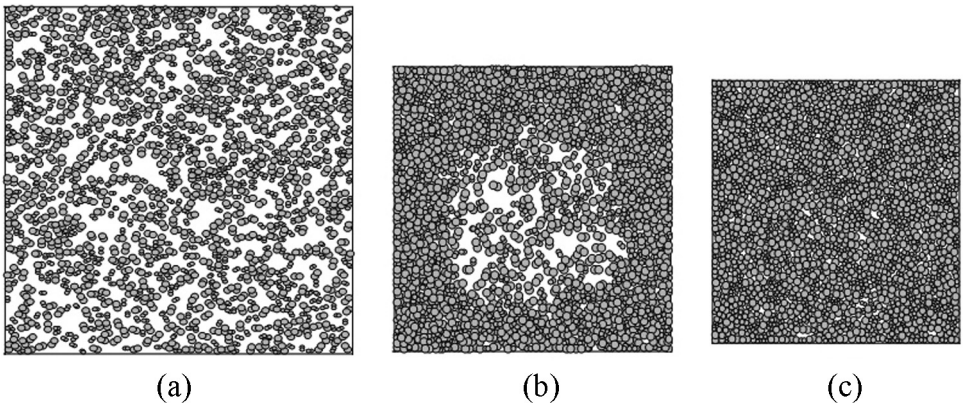


**Fig. 3.** Illustration of the method of isotropic compression (Iso) showing (a) initial particle distribution, (b) isotropic compression in progress, and (c) the final specimen.

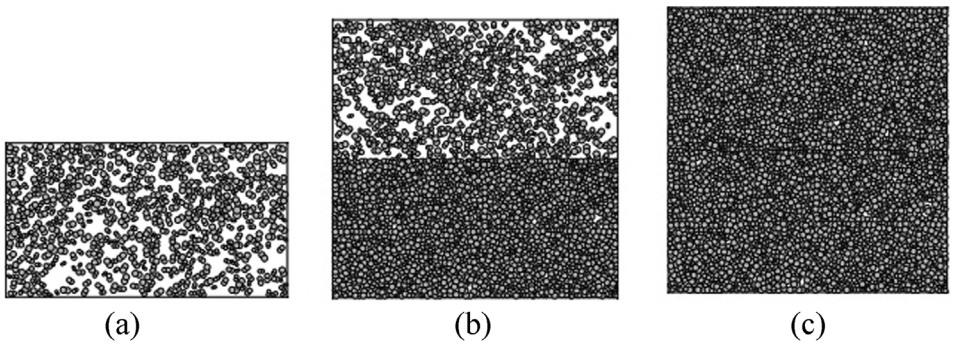


**Fig. 4.** Illustration of the method of multi-layer compression (Mult) showing (a) first-layer compression, (b) third-layer compression, and (c) the final specimen.

of the vessel to compact particles, which are initially in an extremely loose state and almost free of contact forces until the target sample size is attained (Jiang et al., 2003). For multi-layer compression, a specimen is generated in five layers each of the same thickness. For the first layer, particles are randomly generated in a designated area, as shown in Fig. 4(a), and the top boundary wall is then moved downward to compact them until the specified layer height is achieved. After compaction, the top boundary wall is moved upward to leave a void space for generating new particles of the second layer, after which the compaction is once again conducted and this process is repeated five times.

At the end of deposition or compaction, an area of 25 cm × 25 cm is chosen as the specimen for subsequent consolidation and shearing. For computational efficiency, the size of specimens used in DEM simulations is generally smaller than the size of specimens typically used in physical tests; many simulations in the literature have used specimens of similar sizes as that used in this study, or smaller (Jiang et al., 2003; Khalili & Mahboubi, 2014; Masson & Martinez, 2001; Zhang & Thornton, 2007; Gu, Yang, & Huang, 2013). Provided the ratio of specimen size to particle size is properly chosen, the simulations are expected to provide credible results. Consolidation is performed by moving the four rigid boundary walls synchronously inward or outward until the target stress and packing density state is attained. It should be noted that a temporary inter-particle friction coefficient is used in the sample preparation process such that a desired stress and density state can be relatively easily achieved; and is thus, necessarily, obtained by trial and error. The inter-particle friction coefficient should then be restored to the normal value ($\mu_s = 0.5$ in this study) for subsequent consolidation and shearing. All numerical specimens in this study were sheared under drained conditions, implemented by moving the two loading walls in the strain-controlled condition and also maintaining a constant confining stress. A summary of the specimen information is provided in Table 2.

Given that the objective of this study is to investigate the effect of sample preparation and the associated fabric anisotropy, it is important to consider that even for the same sample preparation method, assemblies with different size distributions will exhibit different overall responses (Investigated by Dai et al., 2015). Thus,

**Table 2**
Sample and biaxial test parameters, including preparation method and initial anisotropy.

| Test name | SPM | $p_0$ (kPa) | $e_0$ | *PN* | *CN* | $a_n$ | $\mu_{ini}$ |
|---|---|---|---|---|---|---|---|
| TS-D01 | Dep | 100 | 0.206 | 2149 | 4.64 | 0.167 | 0.185 |
| TS-D02 | | 200 | 0.260 | 2036 | 3.81 | 0.022 | 0.500 |
| TS-D03 | | 500 | 0.203 | 2149 | 4.81 | 0.159 | 0.185 |
| TS-D04 | | 600 | 0.179 | 2194 | 5.27 | 0.184 | 0.100 |
| TS-D05 | | 800 | 0.202 | 2149 | 4.89 | 0.158 | 0.185 |
| TS-M06 | Mult | 100 | 0.206 | 2171 | 4.13 | 0.215 | 0.294 |
| TS-M07 | | 200 | 0.227 | 2171 | 3.83 | 0.210 | 0.500 |
| TS-M08 | | 300 | 0.226 | 2171 | 3.91 | 0.196 | 0.500 |
| TS-M09 | | 500 | 0.203 | 2171 | 4.41 | 0.205 | 0.294 |
| TS-M10 | | 800 | 0.201 | 2171 | 4.56 | 0.201 | 0.294 |
| TS-I11 | Iso | 200 | 0.237 | 2194 | 3.82 | 0.034 | 0.500 |
| TS-I12 | | 200 | 0.166 | 2194 | 5.16 | 0.038 | 0.100 |
| TS-I13 | | 500 | 0.203 | 2194 | 4.35 | 0.041 | 0.280 |
| TS-I14 | | 800 | 0.200 | 2194 | 4.49 | 0.040 | 0.280 |

*Note*: SPM, sample preparation method; *CN*, coordination number; *PN*, particle number; $\mu_{ini}$, friction coefficient prior to consolidation; $a_n$, initial anisotropy; $p_0$, initial confining stress; $e_0$, initial void ratio.

no particle size distribution differences are taken into account in this study so that the focus is on isolating the influence of initial anisotropy only.

*Macroscopic and microscopic indices*

The mean effective stress and deviatoric stress are defined as $p' = (\sigma_1 + \sigma_2)/2$ and $q = \sigma_1 - \sigma_2$, respectively, in which $\sigma_1$ and $\sigma_2$ are the major and minor principal stresses in the biaxial tests. The axial strain is defined as $\varepsilon_a = \Delta L/L$, where $L$ is the original length of the confining wall, and $\Delta L$ is the shortened length resulting from the movement of loading walls. Lateral strain is given as $\varepsilon_r = \Delta R/R$, where $R$ is the initial length of the loading wall, and $\Delta R$ is its reduced length in shear. The volumetric strain is therefore expressed as $\varepsilon_v = \varepsilon_a + \varepsilon_r = \Delta L/L + \Delta R/R$.

The microstructures of a given granular assemblage can be quantified by a fabric tensor formulated from the particle and contact orientations (Oda, 1982, 1999). Taking the contact orientation for example, the second-ranked fabric tensor $F_{ij}$ can be expressed into a continuous form (Rothenburg & Bathurst, 1989) as shown in Eq. (1):

$$F_{ij} = \int_{\Omega} E(n) n_i n_j d\Omega, \tag{1}$$

where $\Omega$ is the representative elemental volume; $n_i$ ($i = 1, 2, 3$) are the direction cosines of the contact unit normal vector **n** with reference to the axes $X_i$ ($i = 1, 2, 3$) in a Cartesian coordinate system (Fig. 5) and $E(n)$ is the probability density function describing the spatial distribution of contact unit normal vectors in a granular assembly. $E(n)$ is defined as shown in Eqs. (2) and (3):

$$E(n) = E_0(1 + d_{ij} n_i n_j), \tag{2}$$

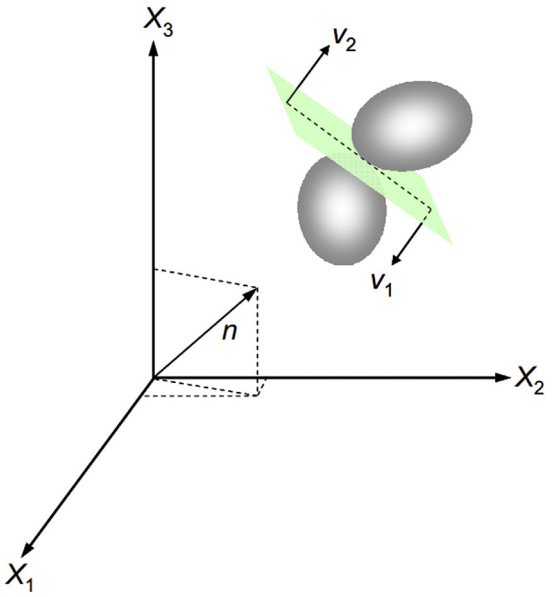


**Fig. 5.** Geometric description of contact unit normal vectors ($\mathbf{v}_1$ and $\mathbf{v}_2$) and a unit vector ($\mathbf{n}$) in a Cartesian co-ordinate system.

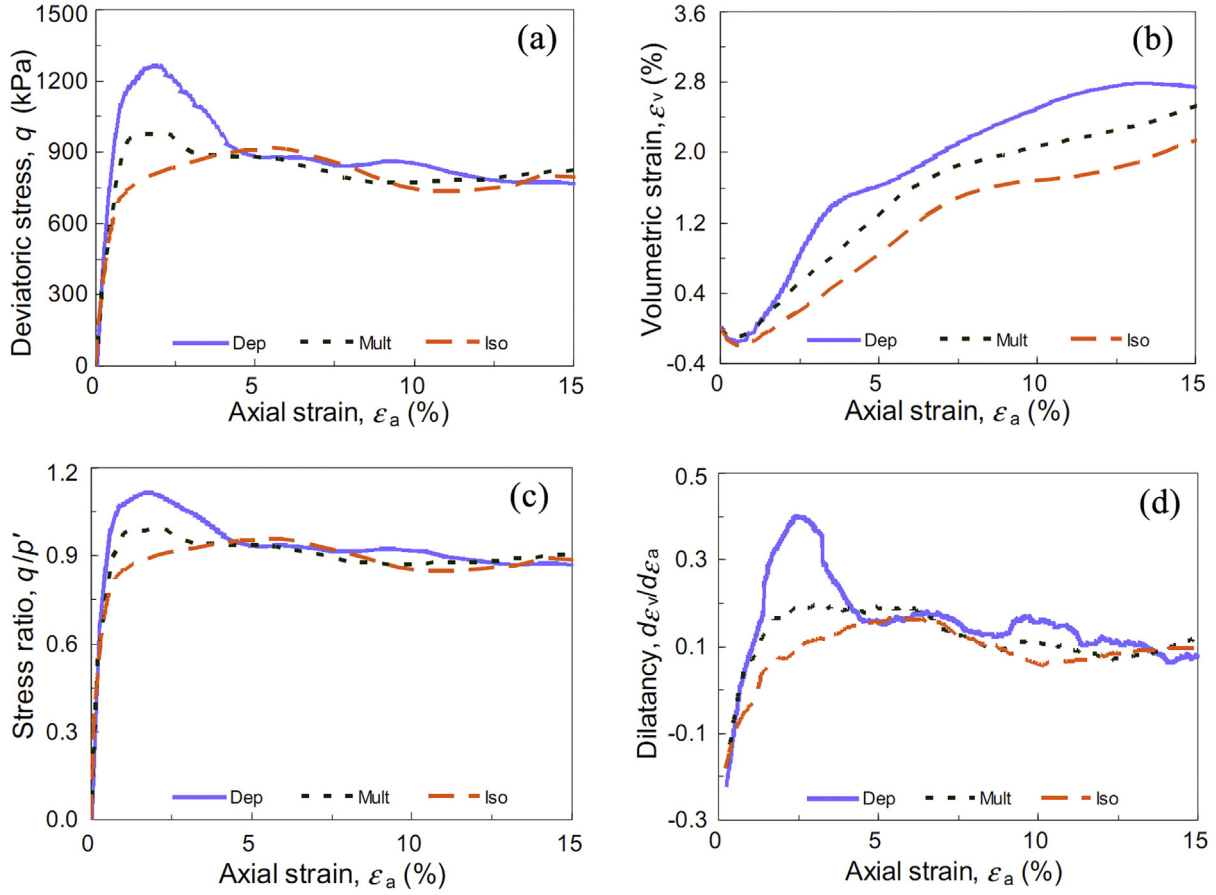


**Fig. 6.** Macroscopic responses of (a) $q$ vs. $\varepsilon_a$, (b) $\varepsilon_v$ vs. $\varepsilon_a$, (c) $q/p'$ vs. $\varepsilon_a$, and (d) $d\varepsilon_v/d\varepsilon_a$ vs. $\varepsilon_a$ for specimens prepared by different methods: TS-D03 (Dep), TS-M09 (Mult), and TS-I13 (Iso) where $p_0 = 500$ kPa and $e_0 = 0.203$.

or

$$E(\phi) = E_0 \left\{1 + a_n \cos\ 2(\phi - \phi_n)\right\}, \quad (3)$$

where $E_0$ is the probability density in an isotropic state; $d_{ij}$ is the second-ranked tensor that estimates the deviation from an isotropic distribution; $\phi$ is direction angle of interest; $a_n$ is the magnitude of fabric anisotropy, and $\phi_n$ indicates the principal direction of fabric anisotropy. The anisotropy parameters $a_n$ and $\phi_n$ are determined as shown in Eq. (4):

$$a_n = \sqrt{d_{11}^2 + d_{12}^2} \quad \text{and} \quad \phi_n = \frac{1}{2} \arctan\left(\frac{d_{12}}{d_{11}}\right). \quad (4)$$

In addition to the anisotropy of microstructures, it is also useful to examine the force anisotropy in a granular assembly. Rothenburg and Bathurst (1989) developed two functions $f(\phi)$ and $t(\phi)$ to characterize the angular variations of the contact normal and tangential force intensities, respectively, as provided in Eqs. (5) and (6):

$$f(\phi) = f_0 \left\{1 + a_f\ \cos\ 2(\phi - \phi_f)\right\}, \quad (5)$$

$$t(\phi) = -f_0 a_t\ \ \sin\ 2(\phi - \phi_t), \quad (6)$$

where $f_0$ is the average contact normal force; $a_f$ is the anisotropy magnitude for the angular distribution of the contact normal force intensities, $\phi_f$ denotes the principal anisotropy direction; and $a_t$ and $\phi_t$ refer to the magnitude and principal direction of anisotropy, respectively, for the angular distribution of the contact tangential force intensities.

The coordination number (CN) is considered an important index for describing the packing of a granular assembly at the microscopic scale. It is conventionally defined as the average contact number per particle. An alternative definition proposed by Thornton (2000), the mechanical coordination number, is adopted here to consider the existence of particles with no contribution to the force transfer in a granular assembly.

## Results and discussion

### *Macroscopic observations*

#### *Shear behavior*

Fourteen biaxial shear test simulations were performed, the parameters of which are summarized in Table 2. The specimens prepared by the multi-layer compression method (Mult) appear to be most anisotropic while those prepared by the isotropic compression method (Iso) are the least anisotropic. Fig. 6 shows the macroscopic responses of the specimens sheared under the same confining pressure ($p_0$ = 500 kPa) and initial void ratio ($e_0$ = 0.203). The specimen prepared by the gravitational deposition method (TS-D03) exhibits the most dilative response, achieving the highest deviatoric stress ($q$), stress ratio ($q/p'$), and dilatancy ($d\varepsilon_v/d\varepsilon_a$) at the peak state. The volumetric strain of this sample is also generally larger than those of the other two samples. The specimen prepared by the isotropic compression method (TS-I13) exhibits the least dilative response, with that prepared by the multi-layer compression method (TS-M09) exhibiting dilatancy in between those of TS-I13 and TS-D03.

It is worth noting that, although these three specimens have the same initial void ratio, their packing states are not exactly the same. The *CN* of TS-D03 is 4.81, higher than those of the other two specimens (TS-M09 = 4.41 and TS-I13 = 4.35). In light of this, the highly

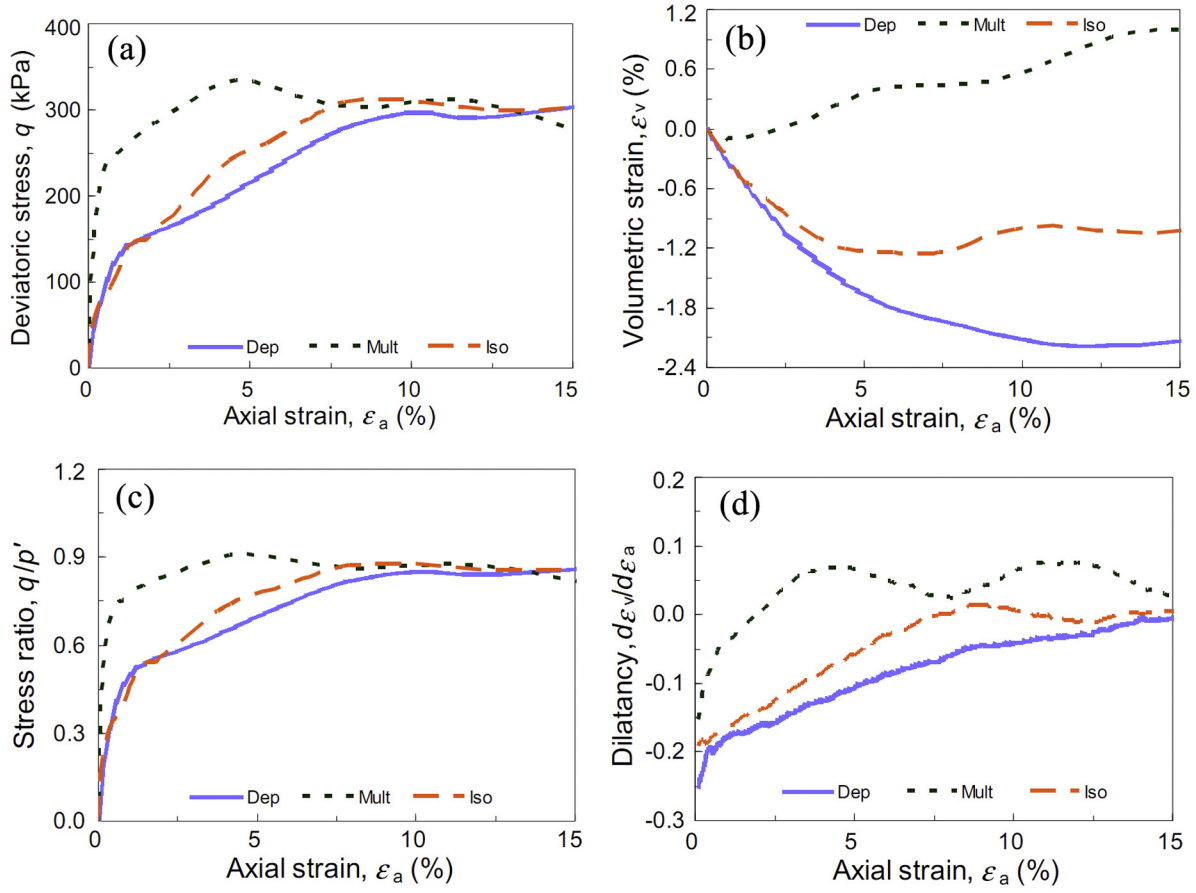


**Fig. 7.** Macroscopic responses of (a) $q$ vs. $\varepsilon_a$, (b) $\varepsilon_v$ vs. $\varepsilon_a$, (c) $q/p'$ vs. $\varepsilon_a$, and (d) $d\varepsilon_v/d\varepsilon_a$ vs. $\varepsilon_a$ for specimens prepared by different methods: TS-D02 (Dep), TS-M07 (Mult), and TS-I11 (Iso) where $p_0$ = 200 kPa and $CN \approx 3.82$.

dilative behavior of TS-D03 cannot be solely attributed to the effects of fabric anisotropy induced by the sample preparation. Nevertheless, compared with TS-I13, the more dilative response of TS-M09 can be largely attributed to the stronger fabric anisotropy in the initial state, as evidenced by its anisotropy index, $a_n$, of 0.205 (Table 2). The anisotropy index of TS-I13 is found to be 0.041, indicating an approximately isotropic state prior to shearing. Regardless of the discrepancies in the packing state and fabric anisotropy in the initial state, all three specimens tend to reach a common critical state with respect to deviatoric stress, stress ratio, and dilatancy at large shear strains. The deviatoric and mean effective stresses of the three specimens at large shear strains are approximately 780 and 890 kPa, respectively, and the void ratios at large shear strains are similar, approximately 0.210. In particular, the dilatancy indices $d\varepsilon_v/d\varepsilon_a$ are around 0.1 at large strains and, equivalently, the dilation angle is $\psi = 3^\circ$, implying a low dilation level close to the critical state where the effect of fabric anisotropy is nearly erased. Fig. 7 presents the macroscopic behavior of another group of test specimens reconstituted by the three preparation methods discussed, which have a confining pressure of 200 kPa and $CN \approx 3.82$ in the initial state. The specimen prepared by the deposition method (TS-D02) and that prepared by isotropic compression (TS-I11) show similarly contractive responses, without any evident peaks in deviatoric stress, stress ratio or dilatancy. As indicated in Table 2, the initial anisotropy index of TS-D02 (0.022) is the lowest, similar to that of TS-I11 (0.034), while that of TS-M07 (0.210) is markedly higher. The difference in $a_n$ values is therefore the main reason why TS-D02 and TS-I11 display similar shear behavior and both are more contractive than TS-M07. The three specimens also all appear to have reached the critical state at large strains. The deviatoric stresses and stress ratios are approximately 300 kPa and 0.82–0.85, respectively, while beyond the strain level $\varepsilon_a = 10\%$. Also, the volumetric strains do not appear to vary at large shear strains and $d\varepsilon_v/d\varepsilon_a$ approaches zero when $\varepsilon_a$ approaches 15%. These observations indicate that the initial fabric anisotropy exerts little impact on the shear behavior at large strains and that the critical state is independent of the initial fabric anisotropy.

The peak stress ratio and peak dilatancy, namely, $(q/p')_{max}$ and $(d\varepsilon_v/d\varepsilon_a)_{max}$, are plotted in Fig. 8 against $a_n$ in the initial state. The peak stress ratio and peak dilatancy appear to positively correlate with $a_n$ given that they increase with increasing $a_n$. This implies that the fabric anisotropy caused by sample preparation exerts a considerable effect on the peak shear strength and peak dilatancy.

*Stress–dilatancy relationship*

To describe the stress–dilatancy behavior of granular soil, Rowe (1962) used the stress–dilatancy equation shown in Eq. (7):

$$\frac{\sigma_1}{\sigma_3(1+d\varepsilon_v/d\varepsilon_1)} = \tan^2\left(\frac{\pi}{4}+\frac{1}{2}\phi_f\right), \quad (7)$$

where $\sigma_1$ and $\sigma_3$ are the axial and radial stresses (major and minor principal stresses) in a conventional triaxial compression test; $\varepsilon_v$ and $\varepsilon_1$ are the volumetric and axial strain; $\phi_f$ is a soil friction angle ranging between the inter-particle friction angle $\phi_\mu$ and the critical state friction angle $\phi_{cs}$.

The stress–dilatancy data in the form of the stress ratio ($q/p'$) versus $d\varepsilon_v/d\varepsilon_a$, are plotted in Fig. 9 to examine their interrelationship. The data points in Fig. 9 correspond to the strain levels at $\varepsilon_a = 0.5\%$, 1.0%, 2.5%, 5.0%, 7.5%, 10%, 12.5%, and 15%. It is observed that the variation of the stress ratio against the dilatancy is not strongly dependent on the effect of the fabric anisotropy generated by the sample preparation and that a correlation exists between the stress ratio and the dilatancy. Furthermore, Eq. (7) reasonably fits the trend, provided that $\phi_f$ takes the value of $\phi_{cs}$ (24.2°). These observations imply that the initial fabric anisotropy does not exert considerable influence on the stress–dilatancy relationship although it does affect the stress ratio and dilatancy separately.

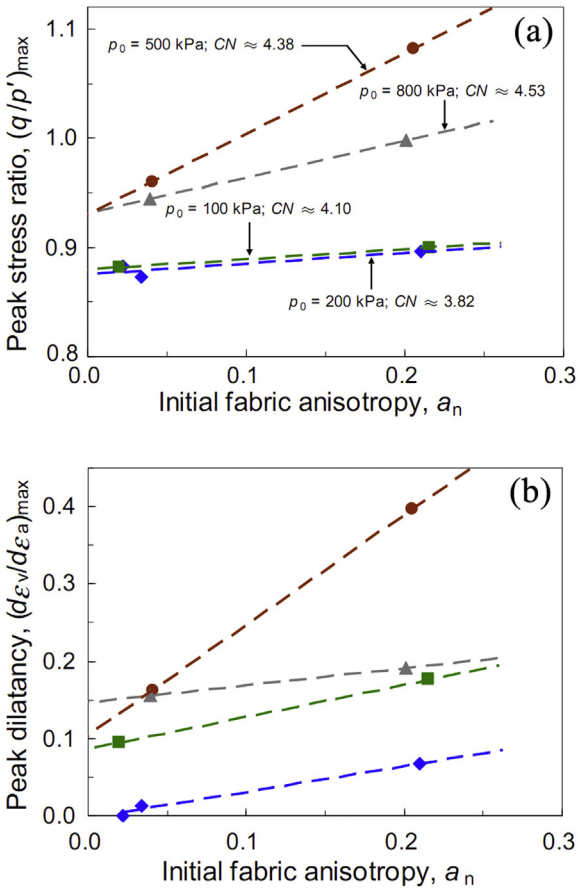


**Fig. 8.** The relationship between (a) the peak stress ratio and initial fabric anisotropy and (b) peak dilatancy and initial fabric anisotropy for varying values of $p_0$ and $CN$.

*Microscopic analysis*

*Fabric anisotropy and coordination number*

The evolution of anisotropy indices $a_n$ and $a_f$ for the specimens shown in Fig. 7 is illustrated in Fig. 10, in which it is evident that $a_n$ and $a_f$ for the specimens prepared by gravitational deposition (TS-D02) and isotropic compression (TS-I11) are similar, a finding

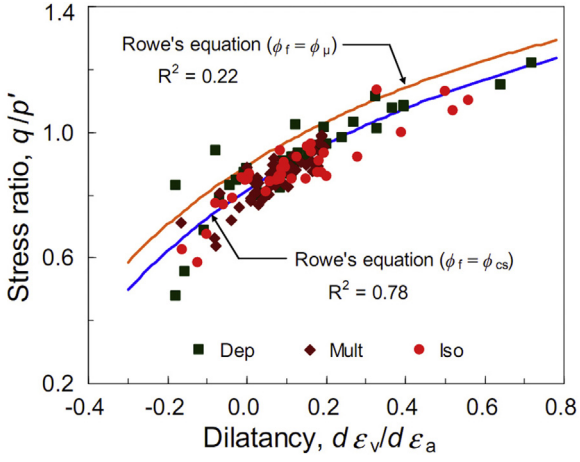


**Fig. 9.** Illustration of the stress–dilatancy relationship $q/p'$ vs. $d\varepsilon_v/d\varepsilon_a$ for the three sample preparation methods (Dep, Mult, and Iso).

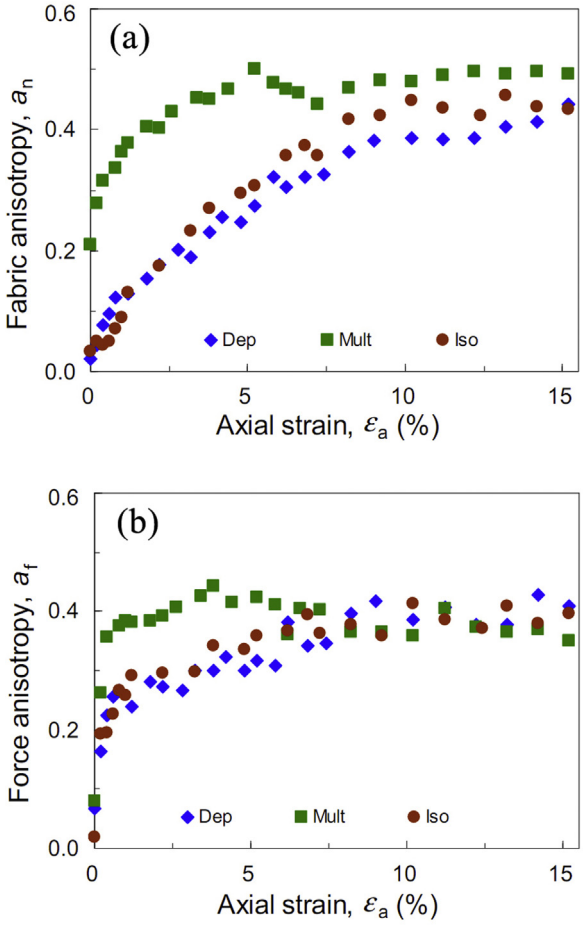


**Fig. 10.** Evolution of anisotropy indices (a) $a_n$ and (b) $a_f$ with increasing axial strain for specimens prepared by different methods: TS-D02 (Dep), TS-M07 (Mult), and TS-I11 (Iso) where $p_0 = 200$ kPa and $CN \approx 3.82$.

consistent with the macroscopic responses. It is also noted that the indices $a_n$ and $a_f$ of TS-M07 are well above those of TS-D02 and TS-I11 when $\varepsilon_a$ is less than 7.5%. However, at large shear strains these three specimens tend to reach a common, stable state. As shown in Fig. 10, the value of $a_n$ at large shear strains is approximately 0.45 and $a_f$ is approximately 0.39. This is supportive of the macroscopic observation of the emergence of the critical state at large shear strains. An alternative observation of the effect of fabric anisotropy is obtained via close scrutiny of rose diagrams describing the angular distribution of the contact unit normal vectors at the initial and critical states, as shown in Fig. 11.

The evolution of *CN*s for specimens prepared with $p_0 = 200$ kPa and $CN \approx 3.82$, as presented in Fig. 12, cannot be differentiated during shearing and all *CN*s experience a slight increase until they reach a common steady value of 3.95 at large shear strains, suggesting that critical state is reached. For the purpose of comparison, the data from another batch of test specimens with the confining stress $p_0 = 500$ kPa and void ratio $e_0 = 0.203$ are also shown in Fig. 12 and it is found that their *CN*s decrease unanimously and arrive at a common steady value of 4.15 at large shear strains.

*Macroscopic and microscopic relationship*

It is well recognized that the macroscopic response of granular soil during shearing is the manifestation of internal particle rearrangements and that the shear strength depends on the fabric and force anisotropy. Rothenburg and Bathurst (1989) proposed a microscopic interpretation of shear strength, as given in Eq. (8), to

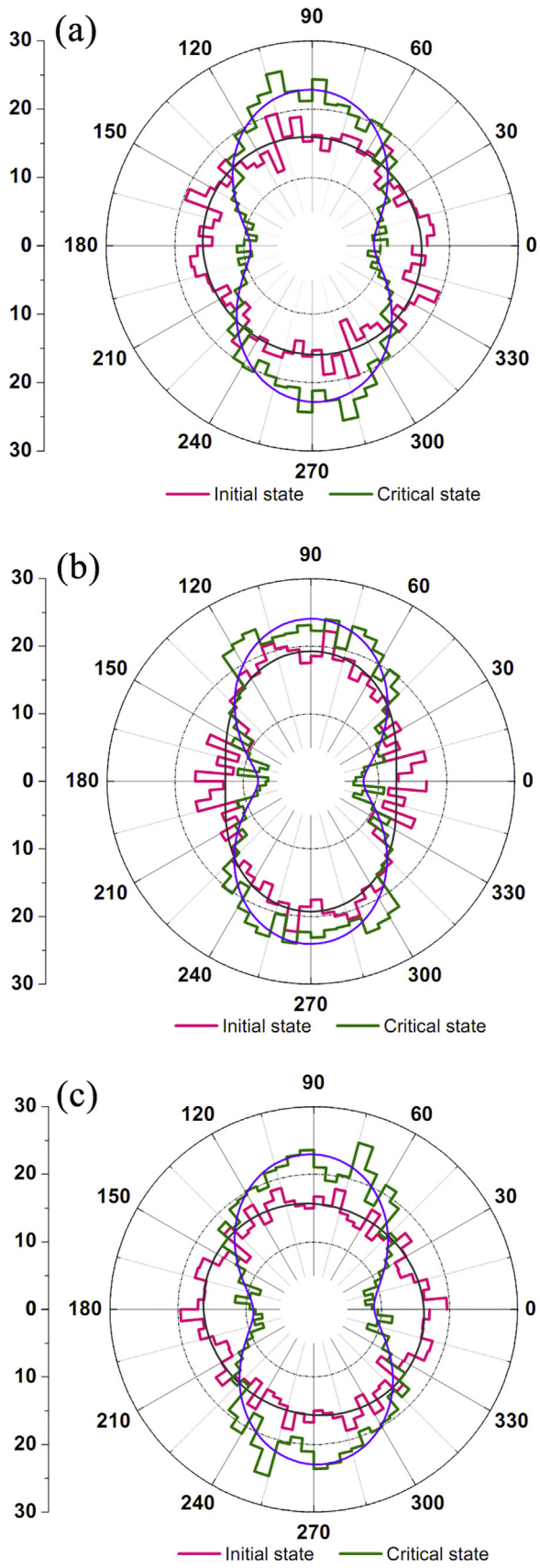


**Fig. 11.** Angular distribution probability densities (%) of the contact unit normal vectors for specimens at the initial and critical states: (a) TS-D02 (Dep), (b) TS-M07 (Mult), and (c) TS-I11 (Iso).

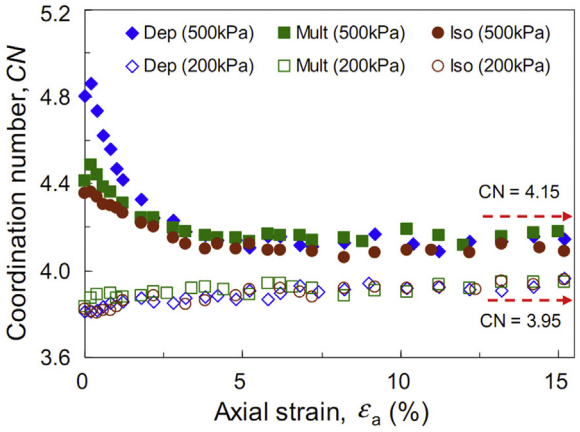


**Fig. 12.** Evolution of the coordination number for various specimen preparation types where parameters for Group I (open symbols) are $p_0 = 200$ kPa and $CN \approx 3.82$ and for Group II (solid symbols) are $p_0 = 500$ kPa and $e_0 = 0.203$.

account for the relationship between the mobilized friction angle $\phi$ and the fabric and force anisotropy indices:

$$\sin\ \phi = \frac{a_n + a_f + a_t}{2 + a_n a_f}. \tag{8}$$

By omitting the product term $a_n a_f$, Eq. (8) can be further simplified into the form of Eq. (9):

$$\sin\ \phi = \frac{a_n + a_f + a_t}{2} \tag{9}$$

At the macroscopic scale, the mobilized friction angle can be defined as a function of principal stresses where $\sin\phi = (\sigma_1 - \sigma_2)/(\sigma_1 + \sigma_2)$. Taking TS-I12 as an example, the mobilized friction angles interpreted with the microscopic and macroscopic expressions are plotted in Fig. 13 against shear strain. It is noteworthy that the mobilized friction angle estimated by the microscopic expression of Eq. (8) is almost identical to that estimated by the principal stresses $\sigma_1$ and $\sigma_2$, while the friction angle given by Eq. (9) is slightly larger than that calculated using Eq. (8).

Fig. 14(a) shows the evolution of the three anisotropy indices $a_n$, $a_f$, and $a_t$. It is observed that the anisotropy indices $a_f$ and $a_t$ both undergo a sharp increase at the start of shearing, and then gradually decrease before entering a steady state. However, $a_n$ undergoes a gradual increase prior to the emergence of a plateau stage where $\varepsilon_a \approx 3.0\%$. Fig. 14(b) shows that the weight contribution of $a_f$ to shear strength, defined as $a_f/(2\sin\phi)$ according to Eq. (9), is highest

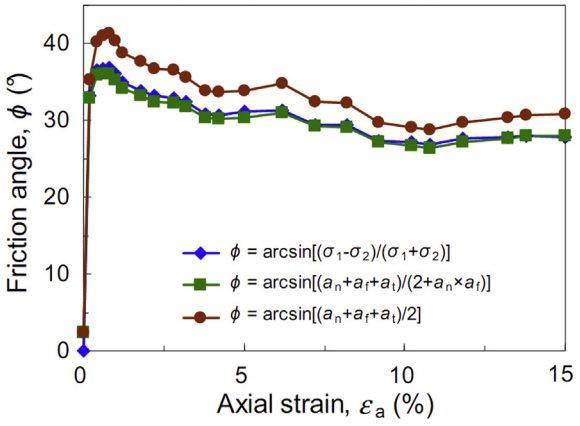


**Fig. 13.** Graphic illustration of the relationship between the mobilized friction angle and axial strain as a function of the fabric and force anisotropy during shear, where $p_0 = 200$ kPa and $e_0 = 0.166$ for specimen TS-I12.

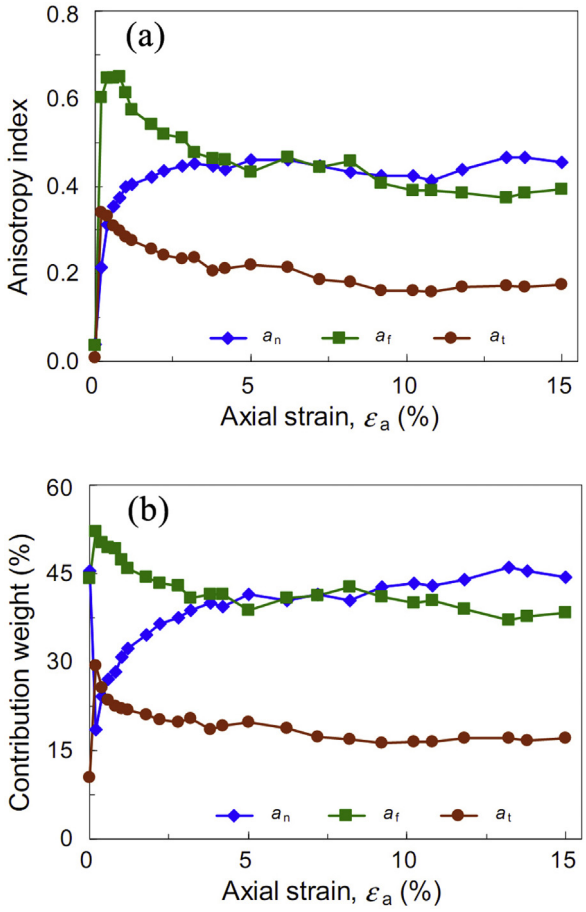


**Fig. 14.** Evolution of (a) the fabric and force anisotropy with increasing axial strain and (b) the weight contribution of fabric and force anisotropy to shear strength, where $p_0 = 200$ kPa and $e_0 = 0.166$ for specimen TS-I12.

in the early shearing stage, with a peak value of approximately 50% at $\varepsilon_a \approx 0.2\%$ and decreasing to approximately 40% at larger shear strains. The weight contribution of $a_n$ decreases sharply to approximately 20% during the initial shearing, and then increases upon further shearing until it arrives at a stable value of approximately 45% at large shear strains. Although the weight contribution of $a_t$ shows an abrupt increase at the start of shearing, it is generally relatively low, and keeps evolving to approximately 17% at large shear strains. Additional test data in Fig. 15 exhibit similar trends and, interestingly, it can be observed that during initial shearing, the weight contribution of $a_n$ for the specimens prepared by multi-layer compression are highest and for those prepared by isotropic compression are lowest. Opposite observations can be obtained in terms of the contribution weights of $a_f$ and $a_t$. The marked discrepancies in the contribution weights of anisotropy indices at the early shearing stage seem to vanish at large shear strains, with the ratio of $a_n$:$a_f$:$a_t$ at 45:38:17. This indicates that the influence of initial inherent fabric anisotropy is almost erased at large shear strains and shear strength is governed by the effect of the stress-induced anisotropy.

To better understand shear strength, it is first necessary to define the stress tensor $\sigma_{ij}$ at the microscopic scale according to Eq. (10) (Oda, 1999):

$$\sigma_{ij} = \frac{1}{v}\sum_{k=1}^{n_c} f_i^k l_j^k, \tag{10}$$

where $v$ is the assembly volume; $n_c$ is the contact number; $k$ is the superscript representing the sequence of contacts; $f_i^k$ is the contact

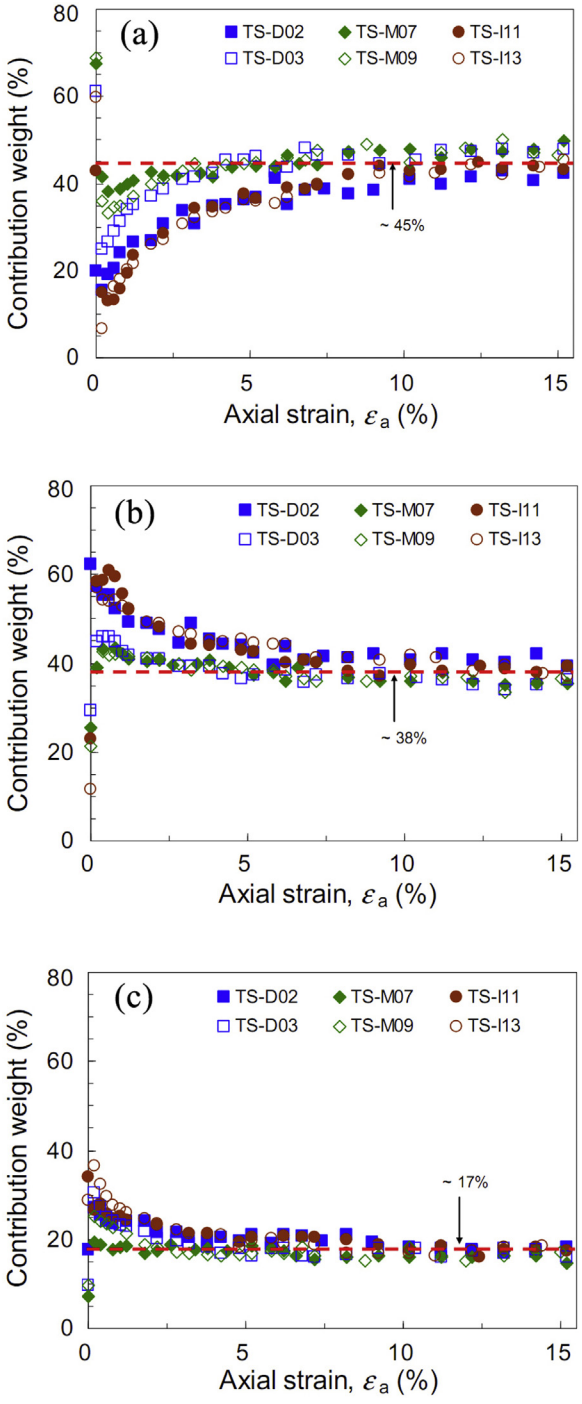


**Fig. 15.** Evolution with axial strain of the weight contribution of (a) $a_n$, (b) $a_f$ and (c) $a_t$.

force vector at the $k$th contact and $l_j^k$ is the branch vector connecting the centroids of the two particles in contact with each other at the $k$th contact. As the contact force vector $f_i^k$ can be decomposed into two sub-parts: the normal force part and tangential force part, Eq. (10) can be rewritten as shown in Eq. (11):

$$\sigma_{ij} = \frac{1}{v}\sum_{k=1}^{n_c}(Nn_i^k + Tt_i^k)l_j^k, \tag{11}$$

where $N$ and $T$ are the intensities of the contact normal and tangential force vectors, respectively; $n_i^k$ is the contact unit normal vector

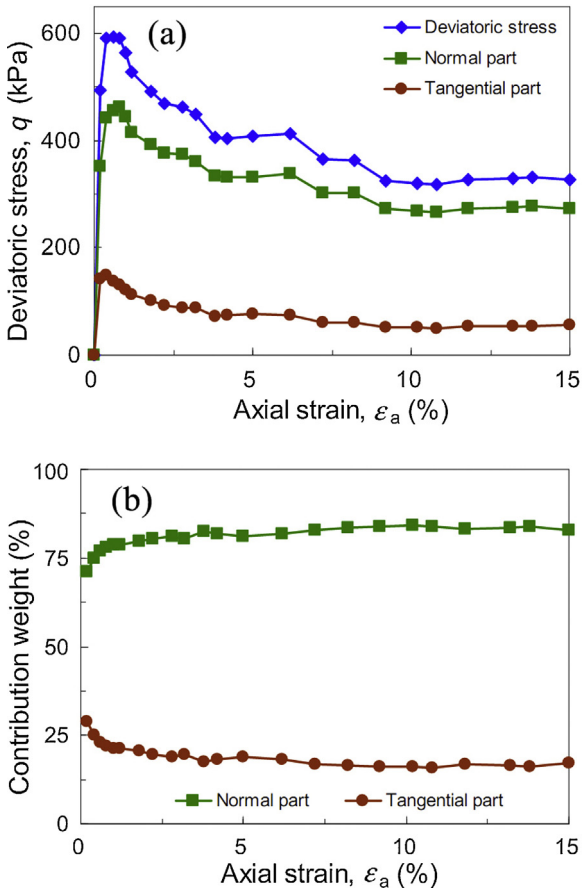


**Fig. 16.** Graphic illustration of (a) the decomposition of deviatoric stress and (b) the weight contribution of the normal and tangential parts against axial strain where $p_0$ = 200 kPa and $e_0$ = 0.166 for specimen TS-I12.

at the $k$th contact and $t_i^k$ is the contact unit tangential vector. It then follows that the stress tensor can be defined as shown in Eq. (12):

$$\sigma_{ij} = \frac{1}{v}\sum_{k=1}^{n_c}Nn_i^k l_j^k + \frac{1}{v}\sum_{k=1}^{n_c}Tt_i^k l_j^k. \tag{12}$$

The decomposed deviatoric stresses of TS-I12 are depicted in Fig. 16(a). It is observed that the contact normal force dominates the contribution to the deviatoric stress, with its weight contribution increasing from approximately 70% in the initial state to above 80% at large shear strains (Fig. 16(b)). Fig. 17 also shows that the contact normal force chains are distinctly stronger than the contact tangential force chains. It can thus be concluded that the deviatoric load is mostly carried by the contact normal force.

*Particle motion*

Fig. 18 presents the relationship between the rotation rate ($d\theta/d\varepsilon_a$) and sliding ratio ($p_s$) and shear strain ($\varepsilon_a$). The rotation rate ($d\theta/d\varepsilon_a$) is a useful index for characterizing particle rolling behavior, where $\theta$ is the average particle rotation angle in radians and, hence, $d\theta/d\varepsilon_a$ is alternatively interpreted as an average incremental rotation angle per an extremely small strain interval. The sliding ratio $p_s$ is defined as the number of sliding contacts at which the mobilized friction coefficient is >0.9999 $\mu_s$ ($\mu_s$: inter-particle friction coefficient), divided by the total contact number of a granular assembly. Fig. 18 shows that the sliding ratio and rotation rate both experience a peak state at an initial shearing stage from $\varepsilon_a$ = 0.0% to $\varepsilon_a$ = 2.5%, regardless of the sample preparation method used. It is also observed that the emergence of the peak rotation

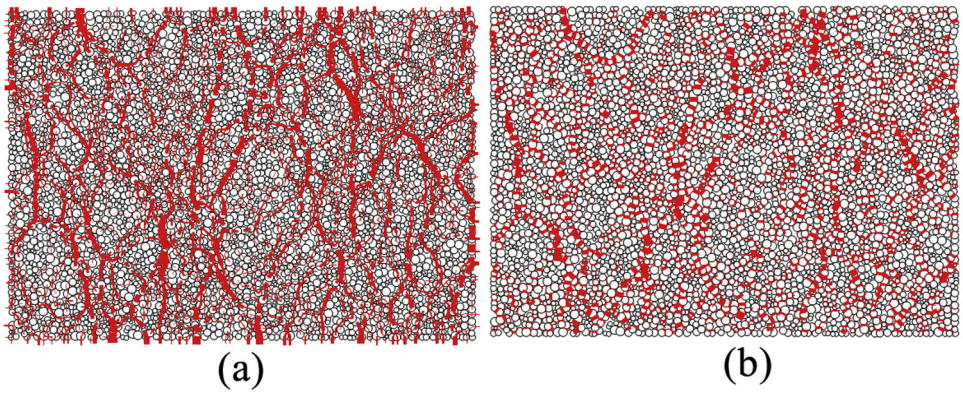


**Fig. 17.** A microscopic view of force chains at $\varepsilon_a$ = 15% showing (a) contact normal force and (b) contact tangential force where $p_0$ = 200 kPa and $e_0$ = 0.166 for specimen TS-I12.

rate and sliding ratio occurs at approximately the same shear strain level as the occurrence of contractive shear responses. It can be inferred that the contractive shear behavior upon the initial shearing is probably accompanied by the most intense particle rearrangements and microstructure reorganization via inter-particle sliding and rolling behavior. Nevertheless, at large shear strains, the rotation rate and sliding ratio seem to reach common steady values of ~2.0 and ~0.04, respectively, implying the critical state is reached from the perspective of microscopic particle motion.

## Discussion

Critical state data points derived from all numerical tests are graphically illustrated as $e$–log $p'$ (Fig. 19(a)) and $q$–$p'$ plots (Fig. 19(b)). A unique CSL exists in the $q$–$p'$ plane and, despite some scatter, a single CSL is also evident in the $e$–log $p'$ plane. These observations suggest that the initial fabric anisotropy has little influence on the position of the CSL.

The uniqueness of the CSL in Fig. 19 is in good agreement with the findings presented in terms of the effects of initial fabric anisotropy induced by sample preparation on other parameters

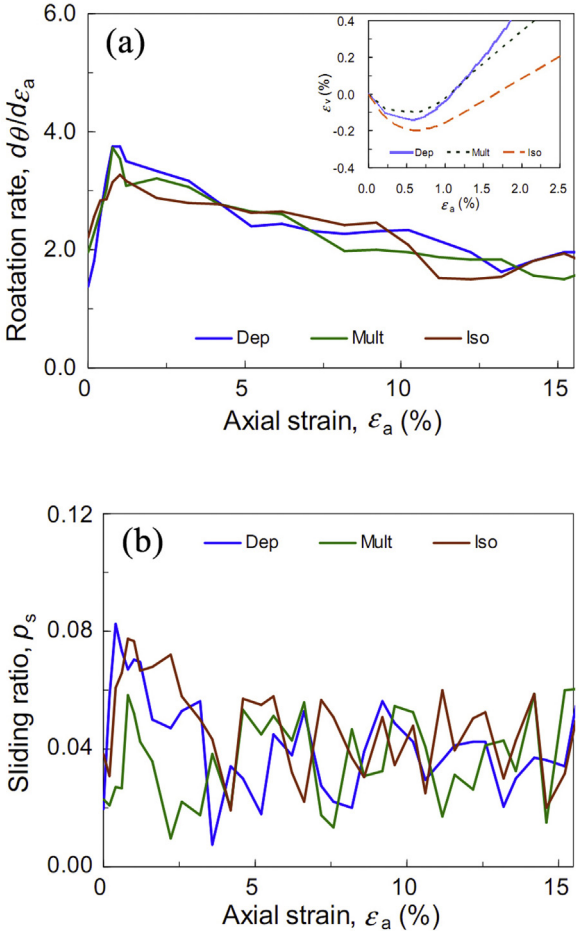


**Fig. 18.** Particle motions showing (a) $d\theta/d\varepsilon_a$ vs. $\varepsilon_a$ and (b) $p_s$ vs. $\varepsilon_a$ where $p_0$ = 500 kPa and $e_0$ = 0.203 for specimens TS-D03 (Dep), TS-M09 (Mult) and TS-I13 (Iso), with the inset in (a) representing $\varepsilon_v$ vs. $\varepsilon_a$ at an initial shearing stage from $\varepsilon_a$ = 0.0% to $\varepsilon_a$ = 2.5%.

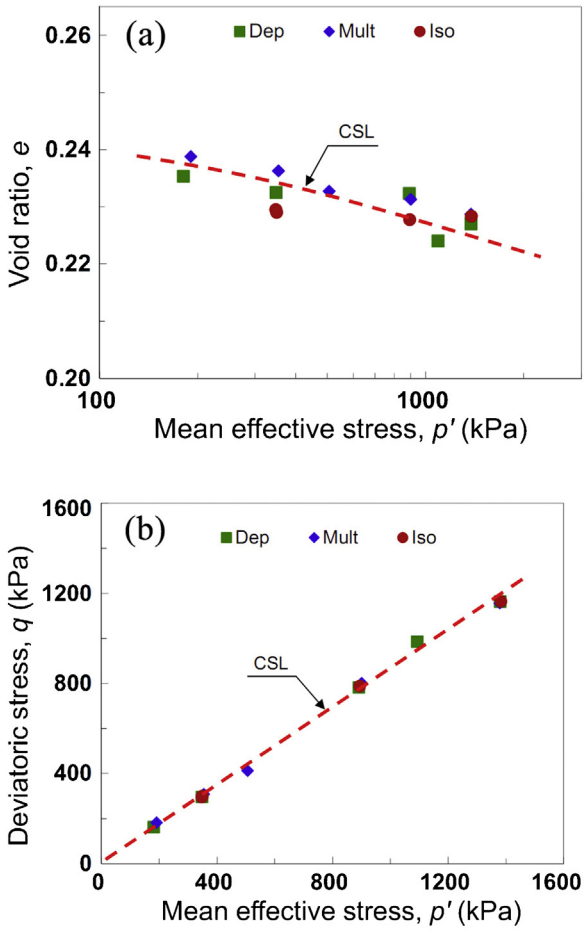


**Fig. 19.** Graphic illustration of the critical state line (CSL) in plots of (a) $e$–log $p'$ and (b) $q$–$p'$ for all specimens prepared by different methods, both illustrating that the initial fabric anisotropy has little influence on the CSL position.

of shear response. In addition to the deviatoric stress, stress ratio, and dilatancy, it has been consistently demonstrated that the anisotropy indices such as $a_n$ and $a_f$, the *CN* and the particle motion indices have each tended to reach an approximately constant value at large shear strains (Figs. 10, 12, 18). The impact of initial fabric anisotropy as a result of sample preparation disappear at large shear strains, and the specimens with different initial fabric anisotropy tend to share a common steady state in terms of macroscopic and microscopic indices.

## Conclusions

A DEM investigation has been conducted to examine the effect of initial fabric anisotropy on the shear behavior of granular soil. The main findings are as follows.

(a) The initial fabric anisotropy resulting from the sample preparation method plays an important role in the shear behavior of granular soil: the more anisotropic the fabric is, the more dilative (or less contractive) the shear behavior is. At large shear strains, the impact of initial fabric anisotropy seems to be eliminated and the specimens prepared by different methods tend to demonstrate a common steady state in terms of deviatoric stress, stress ratio, and dilatancy. The peak stress ratio and peak dilatancy increase concomitantly with the fabric anisotropy index $a_n$.
(b) Initial fabric anisotropy does not strongly affect the stress–dilatancy relationship, and the relationship can be generally described by Rowe's equation provided that the soil friction angle $\phi_f$ is taken to be the critical state friction angle.
(c) The evolution of fabric anisotropy indices $a_n$ and $a_f$ during shear indicates an inclination to arrive at a constant value at large shear strains, irrespective of the sample preparation method. Similarly, the *CN* also reaches an approximately constant value at large shear strains.
(d) The influence of initial inherent anisotropy on the mobilized friction angle seems to disappear at large strains where the ratio of the weight contribution of anisotropy indices $a_n$, $a_f$, and $a_t$ is approximately 45:38:17. The deviatoric load is found to be principally carried by contact normal force rather than contact tangential force.
(e) Both the rotation rate and sliding ratio experience a peak state in the initial shearing stage, indicating that the contractive shear response is generally involved with intense microscopic particle motions. Both the rotation rate and sliding ratio tend to reach a common steady value at large shear strains, which corresponds to the achievement of the critical state.
(f) The initial fabric anisotropy generated by different sample preparation methods exerts little influence on the position of the CSL in plots of both $e$–log $p'$ and $q$–$p'$, which is in good agreement with the evolutionary trends of various macroscopic- and microscopic-scale indices.

## Acknowledgements

The authors gratefully acknowledge the financial support of the National Natural Science Foundation of China (Nos. 51209237, 51428901, 41030747) and the Fundamental Research Funds for the Central Universities (No. 13lgpy05).

## References

Been, K., Jefferies, M. G., & Hachey, J. (1991). The critical state of sands. *Géotechnique, 41*(3), 365–381.
Castro, G. (1969). *Liquefaction of sands* (Doctoral dissertation). Cambridge, USA: Harvard University.
Chang, N., Heymann, G., & Clayton, C. (2011). The effect of fabric on the behavior of gold tailings. *Géotechnique*, *61*(3), 187–197.
Chen, Y., & Chuang, J. (2001). Effects of fabric on steady state and liquefaction resistance. *Proceedings of the Eleventh International Offshore and Polar Engineering Conference*, *2*, 524–529.
Cundall, P. A. (1971). A computer model for simulating progressive, large scale movements in blocky rock systems. In *Proceedings of Symposium of International Society of Rock Mechanics (Vol. 1 Paper No. II-8)* Nancy, France.
Dai, B. B. (2010). *Micromechanical investigation of the behavior of granular materials* (Doctoral dissertation). Hong Kong, China: The University of Hong Kong.
Dai, B., Yang, J., & Luo, X. (2015). A numerical analysis of the shear behavior of granular soil with fines. *Particuology*, *21*, 160–172.
DeGregorio, V. B. (1990). Loading system, sample preparation, and liquefaction. *Journal of Geotechnical Engineering*, *116*(5), 805–821.
Gu, X., Yang, J., & Huang, M. (2013). DEM simulation of the small strain stiffness of granular soils: Effect of stress ratio. *Granular Matter*, *15*, 287–298.
Ishihara, K. (1993). Liquefaction and flow failure during earthquakes. *Géotechnique*, *43*(3), 351–415.
Itasca. (2005). *User's manual for PFC2D*. Minneapolis, USA: Itasca Consulting Group, Inc.
Jiang, M. J., Konrad, J. M., & Leroueil, S. (2003). An efficient technique for generating homogeneous specimens for DEM studies. *Computers and Geotechnics*, *30*, 579–597.
Khalili, Y., & Mahboubi, A. (2014). Discrete simulation and micromechanical analysis of two-dimensional saturated granular media. *Particuology*, *15*, 138–150.
Ladd, R. S. (1974). Specimen preparation and liquefaction of sands. *Journal of Geotechnical and Geoenvironmental Engineering*, *100*(GT10), 1180–1184.
Mahmud Sazzad, M. (2014). Micro-scale behavior of granular materials during cyclic loading. *Particuology*, *16*, 132–141.
Masson, S., & Martinez, J. (2001). Micromechanical analysis of the shear behavior of a granular material. *Journal of Engineering Mechanics*, *127*(10), 1007–1016.
Miura, S., & Toki, S. (1982). A sample preparation method and its effect on static and cyclic deformation-strength properties of sand. *Soils and Foundations*, *22*(1), 61–77.
Muhunthan, B., Masad, E., & Assaad, A. (2000). Measurement of uniformity and anisotropy in granular materials. *ASTM Geotechnical Testing Journal*, *23*(4), 423–431.
Mulilis, J. P., Arulanandan, K., Mitchell, J. K., Chan, C. K., & Seed, H. B. (1977). Effects of sample preparation on sand liquefaction. *Journal of the Geotechnical Engineering Division*, *103*(2), 91–108.
Ng, T.-T. (2004). Macro and micro-behaviors of granular materials under different sample preparation methods and stress paths. *International Journal of Solids and Structures*, *41*, 5871–5884.
Oda, M. (1982). Fabric tensor for discontinuous geological materials. *Soils and Foundations*, *22*(4), 96–108.
Oda, M. (1999). Fabric tensors and its geometrical meaning. In K. Iwashita, & M. Oda (Eds.), *Mechanics of granular materials: An introduction* (pp. 27–35). Rotterdam: A.A. Balkema.
Poulos, S. J. (1981). The steady state of deformation. *Journal of Geotechnical and Geoenvironmental Engineering*, *107*(GT5), 553–561.
Roscoe, K. H., Schofield, A., & Wroth, C. P. (1958). On the yielding of soils. *Géotechnique*, *8*(1), 22–53.
Rothenburg, L., & Bathurst, R. J. (1989). Analytical study of induced anisotropy in idealized granular materials. *Géotechnique*, *39*(4), 601–614.
Rowe, P. W. (1962). The stress–dilatancy relation for static equilibrium of an assembly of particles in contact. In *Proceedings of the Royal Society of London A: Mathematical, Physical and Engineering Sciences (Vol. 269, No. 1339)* (pp. 500–527).
Sadrekarimi, A., & Olson, S. (2012). Effect of sample-preparation method on critical-state behavior of sands. *ASTM Geotechnical Testing Journal*, *35*(4), 548–562.
Sze, H. Y., & Yang, J. (2014). Failure modes of sand in undrained cyclic loading: Impact of sample preparation. *Journal of Geotechnical and Geoenvironmental Engineering*, *140*(1), 152–169.
Tatsuoka, F., Ochi, K., Fujii, S., & Okamoto, M. (1986). Cyclic undrained triaxial and torsional shear strength of sands for different sample preparation methods. *Soils and Foundations*, *26*(3), 23–41.
Thornton, C. (2000). Numerical simulations of deviatoric shear deformation of granular media. *Géotechnique*, *50*(1), 43–53.
Vaid, Y. P., Sivathayalan, S., & Stedman, D. (1999). Influence of specimen-reconstituting method on the undrained response of sand. *ASTM Geotechnical Testing Journal*, *22*(3), 187–195.
Yang, Z. X., Li, X. S., & Yang, J. (2008). Quantifying and modeling fabric anisotropy of granular soils. *Géotechnique*, *58*(4), 237–248.
Yang, J., & Dai, B. B. (2011). Is the quasi-steady state a real behaviour? A micromechanical perspective. *Géotechnique*, *61*(2), 175–184.
Zhang, L., & Thornton, C. (2007). A numerical examination of the direct shear test. *Géotechnique*, *57*(4), 343–354.